scientific reports

Check for updates

OPEN

Eurycomalactone switched hepatocellular carcinoma cells into quiescence through 5′tRF^{Ala}/DVL/β-catenin pathway inhibition

Zhipeng Zhang[1,6], Yanmei Wu[1,6], Wenqiang Liang[1,6], Zhifang Liao[2,3,4], Hongbo Liao[4], Xingxing Xing[2,3], Wenxin Yi[2,3], Zixuan Liu[1,2,5], Yicheng Li[1,2,5], Mengya Shi[1,2,5], Dongling Lin[1], Ting Gu[1], Biao Wu[1], Mingzhi Zou[1]✉, Huilai Miao[1]✉ & Xin Wu[1,2]✉

Although tsRNA has been demonstrated to modulate various physiological processes analogous to miRNA, the potential regulatory functions and mechanisms of tsRNAs related to the pharmacological effects of small molecule drugs remain unclear. Herein, it is shown that eurycomalactone (ELT), a natural product, can reversibly switch hepatocellular carcinoma (HCC) PLC/PRF/5 and HUH7 cells into a quiescent state. This quiescence is characterized by cell proliferation inhibition without cytotoxicity, cell cycle arrest at the G0/G1 phase, and cell reactivation following the removal of ELT. Given the established role of β-catenin activity in mediating cancer cellular quiescence or proliferation, a notable reduction in total, cytoplasmic, and nuclear β-catenin expression, along with its downstream targets Survivin, c-myc, and Cyclin D1, was observed in ELT-treated cells. Subsequently, two new tsRNAs, namely 5′tRF^{Ala} and 5′tiRNA^{Ala}, which match well with the mRNAs of two pivotal upstream regulators (DVL2 and DVL3) of β-catenin based on bioinformatics analyses, were detected to be significantly decreased in ELT-treated PLC/PRF/5 cells using Arraystar small RNA microarray analyses. Consistently, the concentrations of the DVL2 and DVL3 proteins were also found to be reduced by ELT. The mimic of 5′tRF^{Ala} could increase the relative expression of DVL2 and DVL3 mRNA and rescue their decrease induced by ELT, while the mimic of 5′tiRNA^{Ala} could not. It therefore seems that ELT could down-regulate the expression of 5′tRF^{Ala}, leading to the suppression of DVL2 and DVL3 mRNA translation, consequently inhibiting the β-catenin signaling pathway and reversibly switching HCC cells into a quiescent state. Conclusively, our findings imply that tsRNAs, like miRNAs, might activate the translation of their matched mRNAs in non-dividing cells and provide a possible potential for repressing tumor cell growth, although further evidence is still needed.

Keywords Eurycomalactone, tsRNA, 5′tRF^{Ala}, Wnt/β-catenin pathway, Hepatocellular carcinoma cell

Small non-coding RNAs (sncRNAs) are typically less than 200 nucleotides (nt) in length[1]. As the term implies, most of these do not appear to encode proteins[2,3]. Over the last two decades or so, various types of sncRNAs have been identified, including transfer RNAs (tRNAs)[4], circular RNAs (circRNAs)[5], microRNAs (miRNAs)[6], piwi-interacting RNAs (piRNAs)[7], small interfering RNAs (siRNAs)[8], small nucleolar RNAs (snoRNAs)[9], and small nuclear RNAs (snRNAs)[10]. A substantial body of research has demonstrated the close relationship between sncRNAs and various cancers. Indeed, sncRNAs could regulate the occurrence and development of tumors by

[1]The Medical Interdisciplinary Science Research Center of Western Guangdong, The Second Affiliated Hospital of Guangdong Medical University, 524003 Zhanjiang, Guangdong Province, People's Republic of China. [2]Dongguan Key Laboratory of Characteristic Research and Achievement Transformation of Integrated Chinese and Western Medicine for Prevention and Treatment to Common Diseases, First Dongguan Affiliated Hospital, Guangdong Medical University, 523106 Dongguan, Guangdong Province, People's Republic of China. [3]Marine Biomedical Research Institute, Guangdong Medical University, 524023 Zhanjiang, Guangdong Province, People's Republic of China. [4]Guangdong Provincial Key Laboratory of Research and Development of Natural Drugs, School of Pharmacy, Guangdong Medical University, 523808 Dongguan, Guangdong Province, People's Republic of China. [5]Southern Marine Science and Engineering Guangdong Laboratory (Zhanjiang), 524023 Zhanjiang, Guangdong Province, People's Republic of China. [6]Zhipeng Zhang, Yanmei Wu and Wenqiang Liang have contributed equally to this work and shared first authorship ✉email: zmzgdmu@163.com; miaohl-gdwk@gdmu.edu.cn; woodbirdlhb@163.com

influencing numerous key processes, including proliferation signal transduction, cell cycle regulation, apoptosis, epigenetic inheritance, and protein expression[11–13]. tRNAs, which have total lengths of 70–87 nt, are the most common and earliest reported sncRNAs and are found in all organisms[14]. The fundamental function of tRNA is regarded as transporting amino acids[15,16]. A multitude of studies indicates that the dysregulation and mutation of tRNA, and its corresponding protein, are related to the pathogenesis of cancers[17–19]. Furthermore, emerging evidence suggests that tRNA can be further broken down into heterogeneous populations of smaller sncRNAs, designated as tRNA-derived small RNAs (tsRNAs), including tRNA-derived stress-inducing RNAs (tiRNAs) and tRNA fragments (tRFs)[20]. tiRNAs are generated by ANG cleavage of the anticodon loop of mature tRNA, with a length of approximately 31–40 nt[21]. tiRNAs can be categorized as either 5'-tiRNA or 3'-tiRNA, depending on whether they contain 5' or 3' sequences at the cleavage site in the anticodon region[22]. tRFs are approximately 14–30 nt in length and are derived from mature tRNAs or precursor tRNAs. They can also be classified according to their corresponding positions on tRNAs[23]: (1) tRF-1 is derived from the cleavage of the 3' end of pre-tRNAs and contains a polyU sequence, also known as 3'u tRF[24]; (2) tRF-2 is derived from the anticodon loop under hypoxic stress[25]; (3) tRF-3 is generated by the cleavage of the TψC loop of mature tRNA by Dicer and ANG and can be further classified into tRF-3a (18 nt) and tRF-3b (22 nt) based on its length[26]; (4) tRF-5 is produced by cleavage of the D loop, D stem, or 5' half of the anticodon stem of mature tRNA. It can be classified into three subtypes: tRF-5a (14–16 nt), tRF-5b (22–24 nt)and tRF-5c (28–30 nt)[27]; (5) i-tRF is derived from the internal region of mature tRNAs. According to the different cleavage sites, it can also be classified into three subtypes: A-tRF, D-tRF, and V-tRF[28]. The precise mechanisms through which tsRNAs exert their biological functions are still not well understood. However, an increasing amount of evidence from various studies suggests that they have a significant impact on mRNA silencing, stress granule formation, inhibition of apoptosis, translation regulation, epigenetic regulation, and cellular communication[29–32].

The first identification of tsRNAs occurred in the 1970s, at which time they were regarded as mere random degradation products of tRNA with no discernible biological functions[33]. These perceptions were revised following the publication of a study in 2009, which reported that tRF-1001 promoted the proliferation of pancreatic cancer cells[34]. Subsequently, aberrant tsRNA expression has been detected in numerous human diseases due to the acquisition of high-throughput small RNA-Seq and CLIP-Seq data[35]. In particular, dysregulated tsRNA expression has been correlated with the onset and progression of various cancers, including hepatocellular carcinoma (HCC)[36,37]. For instance, Zhan et al.[38] discovered that tRF-Gln-TTG-006 was markedly elevated in the serum of individuals with liver cancer. The proliferative function of this tsRNA was subsequently validated through a series of bioinformatics, colony formation, and cell apoptosis experiments. Kim et al.[39] showed that tRF-LeuCAG can inhibit RPS28 mRNA translation, thereby impeding the process of pre-18s ribosomal RNA and subsequently restraining protein synthesis and inhibiting in situ tumor growth in murine HCCs. Zhu et al.[40] concluded that individuals with hepatocellular carcinomas (HCCs) displayed markedly elevated levels of four tsRNAs in plasma exosomes. The identified tsRNAs were tRNA-ValTAC-3, tRNA-GlyTCC-5, tRNA-ValAAC-5, and tRNA-GluCTC-5. This finding suggests that plasma exosomal tsRNA may be a valuable biomarker for disease detection and thus facilitate treatment.

Although tsRNA has been reported to modulate various biological processes similar to miRNA[28,41,42], it is not clear whether tsRNAs have regulatory functions or mechanisms related to the pharmacological effects of small molecules. In this article, we report that the small molecule eurycomalactone (ELT) (Fig. 1A), a natural product isolated from the roots of *Eurycoma longifolia*[43], can dramatically inhibit cell proliferation without causing cell death. This is achieved by blocking the cell cycle at the G0/G1 phase and reducing the protein biomarkers of PCNA/CDK4/CDK6 in HCC PLC/PRF/5 and HUH7 cells. Following the cessation of ELT treatment, cell growth was observed to reactivate. Given that β-catenin activity influences the proliferation or quiescence of colorectal cancer cells[44], the β-catenin signaling cascade was then studied to establish the mechanism by which ELT exerts such effects. The results revealed that the contents of total cytoplasmic and nuclear β-catenin, as well as those of its target proteins, namely Survivin, c-myc, and Cyclin D1, were all significantly diminished by the administration of ELT. The Arraystar small RNA microarray and bioinformatics analyses were then performed on the total RNA solution extracted from PLC/PRF/5 cells following ELT treatment. And an overexpression experiment by tsRNA mimics was conducted to discuss the potential relationship between tsRNAs and the β-catenin signaling pathway.

Materials and methods

General reagents

Dulbecco's Modified Eagle's Medium (DMEM), phosphate-buffered saline (PBS), fetal bovine serum (FBS), and penicillin-streptomycin were purchased from Gibco Invitrogen (Grand Island, NY, USA). 3-(4,5-Dimethylthiazol-2-yl)-2,5-diphenyl tetrazolium bromide (MTT), right inferior pulmonary artery lysis buffer (RIPA), protein marker (molecular weight 10–180 kD), BeyoECL Star, cell cycle analyses kits, AnnexinV-FITC apoptosis detection kits, 0.1% crystal violet, BeyoClick™ EdU cell proliferation kit, and Hoechst 33342 were purchased from Beyotime Biotechnology (Shanghai, China). Dimethyl sulfoxide (DMSO) and 4% paraformaldehyde (PFA) were purchased from Solarbio (Beijing, China). Trizol was purchased from Thermo Fisher Scientific (Waltham, Massachusetts, USA). Antibodies of DVL2, DVL3, CyclinD1, Survivin, β-catenin, c-myc, CDK4, PCNA, and Tubulin were all purchased from SAB Signalway Antibody (College Park, Maryland, USA). The antibody of CDK6 was purchased from Cell Signaling Technology (Danvers, MA, USA), and Histone H3 was obtained from Santa Cruz Biotechnology (Dallas, Texas, USA). A rtStar™ tRF&tiRNA pretreatment kit and a rtStar™ First-Strand cDNA Synthesis kit (3' and 5' adaptor) were both obtained from Arraystar Inc. (Key West Avenue, Florida, USA).

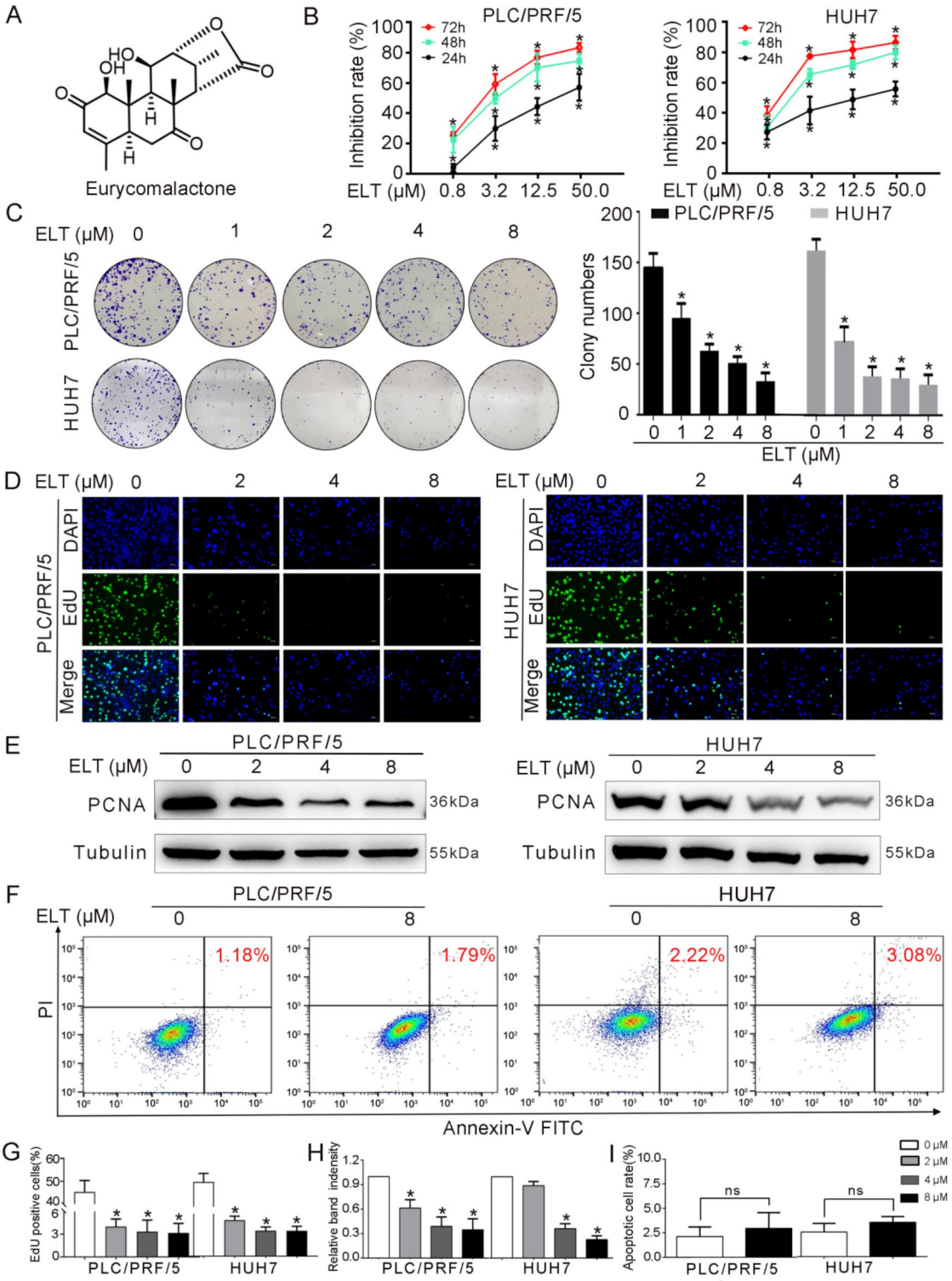

Fig. 1. ELT inhibited the proliferation of PLC/PRF/5 and HUH7 cells without causing cell death. (**A**) The molecular structure of ELT. (**B**) The cell growth inhibition of ELT at various concentrations for 24, 48, and 72 h, respectively, by MTT assay. (**C**) Images of the colony formation following a 14-day exposure to various concentrations of ELT. (**D**) Images of cell cultures after a 48 h ELT treatment followed by an EdU proliferation assay. Scale bars, 100 μm. (**E**) The protein level of PCNA in two cell lines after being treated for 48 h with ELT at various concentrations by Western Blotting. Original blots were presented in Supplementary Fig S3. (**F**) The Annexin V/PI staining of cells after treating with ELT at 8 μM in 6-well plates for 48 h. (**G**-**I**) The statistical analyses of the EdU positive cells, protein level of PCNA, and apoptosis cell rate. The data derived from three separate experiments were displayed as the average ± SD, *, $p < 0.05$, ns, $p > 0.05$.

Cell culture
Human hepatocellular carcinoma (HCC) cell lines, PLC/PRF/5 and HUH7, were procured from the Chinese Academy of Sciences Cell Bank in Shanghai, China. Dulbecco's modified Eagle's medium (DMEM) was used to incubate these cells, enriched with 10% (v/v) fetal bovine serum, and incubated at a temperature of 37 °C in an atmosphere of 5% CO_2 and 95% relative humidity. Cell passage was initiated once the cell density reached approximately 80–90%.

Cell translation
PLC/PRF/5 cells were seeded into 6-well plates and grown for 12 h. The synthetic single-strand mimic of tsRNA and corresponding negative control (Ribobio, Guangzhou, China) were transfected into the cells using Lipofectamine 2000 (Invitrogen) according to the manufacturer's instructions, followed by adding 8 μM ELT and incubating accordingly. tRF5-26-AlaAGC-13: GGGGAATTAGCTCAAGCGGTAGAGCG; 5'tiRNA-36-AlaAGC-10: GGGGAATTAGCTCAAGTGGTAGAGCGCTTGCTTAGC. A scrambled sequence was used as a negative control.

Cell proliferation and cytotoxicity assay
Cells were inoculated into 96-well plates and grown for 12 h, followed by adding ELT at various concentrations and incubating accordingly. Next, MTT was added to each well for a further 4 h. Finally, the liquid in each well was replaced with DMSO. Microplate readers were used to measure the absorbance values of the solutions in the wells at 570 and 630 nanometers, respectively.

Colony formation assay
Cells were inoculated into 96-well plates and cultured for 12 h. A medium supplemented with various concentrations of ELT was given to the cells cultured for a further 24 h after the original medium was removed. Next, the cells were maintained for another 14 days in a medium without ELT. All cell colonies were washed 3 times with PBS, followed by fixation with a 4% PFA solution. Finally, the colonies were stained with a 0.1% solution of crystal violet and photographed. The enumeration of the colonies was conducted using the Image J software for analyses.

EdU staining assay
Experimental protocols were followed according to the manufacturer's guidelines. Cells were exposed to an EdU staining solution for 2.5 h. Next, the stained cells were fixed with 4% PFA, followed by staining with Hoechst 33342. The cells were photographed by a fluorescence microscope.

Hoechst 33,342/PI double staining assay
Cells were treated with 8 μM ELT for 72, 120, and 168 h. Following the required incubation periods, cells were subjected to Hoechst 33342 staining for 30 min. Propidium iodide (PI) was introduced to the cells for an additional 10-min incubation. Stained cells were imaged using fluorescence microscopy.

Flow cytometric analyses of cell apoptosis
The apoptotic cells were assessed using the Annexin V-FITC/PI apoptosis detection kit. Initially, cells were inoculated into 6-well plates and cultured for 12 h. Then, the cells were exposed to a range of ELT concentrations for 48 h. After treatment, the cells were collected, rinsed twice with PBS, and re-suspended in Annexin-V binding buffer. They were subsequently incubated with the Annexin V-FITC/PI staining solution for 20 min. The stained cells were analyzed using a BD FACSCelesta flow cytometer, and the data were processed with FlowJo analytical software.

Flow cytometric analyses of the cell cycle
Cells were inoculated into 6-well plates and grown for 12 h, after which they were exposed to ELT for a further 24–48 h. Subsequently, the cells were suspended in 70% ethanol and stored overnight at a temperature of 4 °C. Following this, the cell cycle distribution was determined through the application of flow cytometry techniques. The ModFit LT software was utilized to quantify the proportions of cells present in the G0/G1, S, and G2/M phases of the cell cycle.

Western blotting assay
Cells were inoculated into culture dishes and grown for 12 h. Following this, various concentrations of ELT were added and the incubation continued for the requisite time. Total protein was extracted using RIPA lysis buffer with 100 mM PMSF. Separation of cytoplasmic and nuclear protein fractions was performed utilizing an extraction kit. The protein concentration within the lysates was quantified using a BCA protein assay. An equal volume of protein samples was applied to SDS-PAGE gels for protein separation. Subsequently, the resolved proteins were transferred onto PVDF membranes at a voltage of 80 volts for 90 min. The membranes were blocked with 5% skim milk in TBST for 2 h, followed by overnight incubation with the respective primary antibodies at 4 °C. After washing with TBST, the membranes were treated with HRP-tagged secondary antibodies specific to rabbit or rat for 2 h at room temperature. An electrochemiluminescence (ECL) system was used to visualize the bands.

Arraystar small RNA microarray analyses
RNA was isolated from each sample by the Trizol method and mixed in three cell culture dishes to minimize potential errors. The concentration of RNA was measured with a NanoDrop ND-1000 spectrophotometer, while its integrity was assessed using either a Bioanalyzer 2100 or agarose gel electrophoresis under denaturing

conditions. For the small RNA microarray analyses by Arraystar, 100 ng of RNA was dephosphorylated at 37°C for 40 min with 3× T4 polynucleotide kinase. This process involved the removal of phosphoric (P) and cyclic phosphoric (cP) chemical groups at the 3' end of the RNA, resulting in the formation of the 3-OH end. The reaction was inactivated at 70 °C for 5 min and then quickly chilled to 0 °C. After the addition of 7 µL DMSO, the RNA was denatured at 100 °C for 3 min and rapidly chilled to 0 °C. The 5' ends of the RNA were labeled with pCp-Cy3 at 16 °C overnight in a solution containing ligase buffer, BSA, and T4 RNA ligase. The labeled RNA was then hybridized with the hybridization buffer at 100 °C for 5 min before being chilled to 0 °C. The hybridization of the 45 µL labeled RNA sample to the microarray was carried out at 55 °C for 20 h. Slides were first washed in 6× SSC with 0.005% Triton X-102 for 10 min, followed by a second wash in 0.1× SSC with 0.005% Triton X-102 for 5 min. Sample mixtures were scanned using an Agilent G2505C microarray scanner, and the images were processed with Agilent Feature Extraction software (version 11.0.1.1). The data underwent log2 transformation and normalization. Only samples with probe signals marked as Present (P) or Marginal (M) by the quality control metrics were considered for further analyses. The differential expression of tsRNAs was determined by comparing the fold change (FC) and statistical significance (p-value) between the two groups. Hierarchical clustering and volcano plots were created using R software for visualization.

RNA isolation, reverse transcription, and real-time RT-PCR

Isolation of total RNA from cell samples was performed using Trizol. The rtStar™ tRF&tiRNA pre-treatment and rtStar™ first-strand cDNA synthesis kits (3' and 5' adaptor) were employed for the reverse transcription of RNA into complementary DNA (cDNA), adhering to the protocol outlined by the kit's manufacturer. RT-qPCR was executed with U6 serving as a reference gene. The relative expression levels of tRF were determined using the 2-ΔΔCt method. Real-time RT-PCR for the DVL2 and DVL3 genes (Guangzhou ReGene Biotechnology Co., Ltd.) was performed using the SYBR Green method. GAPDH (Sangon Biotech, Shanghai) served as a reference gene. The primer sequences were presented in Table S1 of the Supporting Information (SI).

Target prediction

The TargetScan software (http://www.targetscan.org) was employed to forecast the probable binding sites of the mRNAs. This process involved identifying conserved 8- and 7-mer sequences that corresponded to the seed regions of the respective mRNAs. Additionally, the miRanda algorithm (http://www.microrna.org) was deployed to anticipate the mRNA targets of the differentially expressed tsRNAs. The overlap of predictions from both methods was considered as the final result in terms of identifying the targeted genes. The miRanda algorithm was used to predict the combination ability of tsRNA with its target gene based on structural analyses and free energy scores. A higher structure score and lower free energy score indicated more accurate target gene predictions. TargetScan software and the miRanda algorithm analyses were based on the original sequences obtained from the Arraystar small RNA microarray analyses.

GO and KEGG pathway analyses of target genes

The genes that were computationally predicted as targets underwent GO analyses. This analyses encompasses three primary categories: biological processes (BP), cellular components (CC), and molecular functions (MF). Fisher's exact test was applied to assess whether there was a statistically significant overlap between the differentially expressed genes and the GO-annotated gene list. GO terms achieving a p-value < 0.05 were interpreted as being significantly enriched. Furthermore, KEGG pathways associated with the target genes were retrieved from the KEGG database. Pathways with a p-value < 0.05 were deemed to be significantly enriched.

Statistical analyses

Statistical analyses were conducted utilizing the GraphPad Prism version 6.0. A Student's t-test was applied to compare the data between the two groups. A p-value < 0.05 was considered statistically significant.

Results

ELT inhibits HCC cell proliferation without causing cell death

Cell proliferation assays were conducted on PLC/PRF/5 and HUH7 cells in vitro after ELT was administered to the cells. The results showed that HCC cell proliferation was markedly suppressed by ELT in a dose- and time-dependent manner (Fig. 1B). ELT significantly reduced the number of colonies formed by these two HCC cell lines in a dose-dependent manner (Fig. 1C). The EdU assay demonstrated that ELT effectively reduced the count of EdU-positive cells in HCC cell lines (Fig. 1D and G). Furthermore, the Western blotting test results revealed that the levels of PCNA protein were sharply depressed by ELT treatment (Fig. 1E and H). However, as revealed by flow cytometric analyses, ELT did not induce cell apoptosis or death in the two cell lines, even after the 48 h exposure to a drug concentration of 8 µM (Fig. 1F and I). This remained the case after 72 h, 120 h, and 168 h (Fig. S1), as evident from conducting a Hoechst 33342/PI double-staining assay. Interestingly, the proliferation of the two cell lines was observed to resume immediately after the cessation of ELT dosing (Fig. S2). This implies that ELT could inhibit the proliferation of HCC cells but did not induce cell death.

ELT induces cell cycle arrest at the G0/G1 phase in HCC cells

After exposing PLC/PRF/5 and HUH7 cell lines to different concentrations of ELT for periods of either 24–48 h, the alterations in their DNA contents at distinct points in the cell cycle were ascertained through the utilization of established techniques. The results, as depicted in Fig. 2A and B, demonstrated that treatment with ELT for 24 h and 48 h markedly induced cell cycle arrest at the G0/G1 phase in the two cell lines, following a concentration-dependent manner. Furthermore, the proteins CDK4 and CDK6, which are related to the G0/G1 phase, were found to be significantly down-regulated as determined by Western blotting (Fig. 2C and D). These

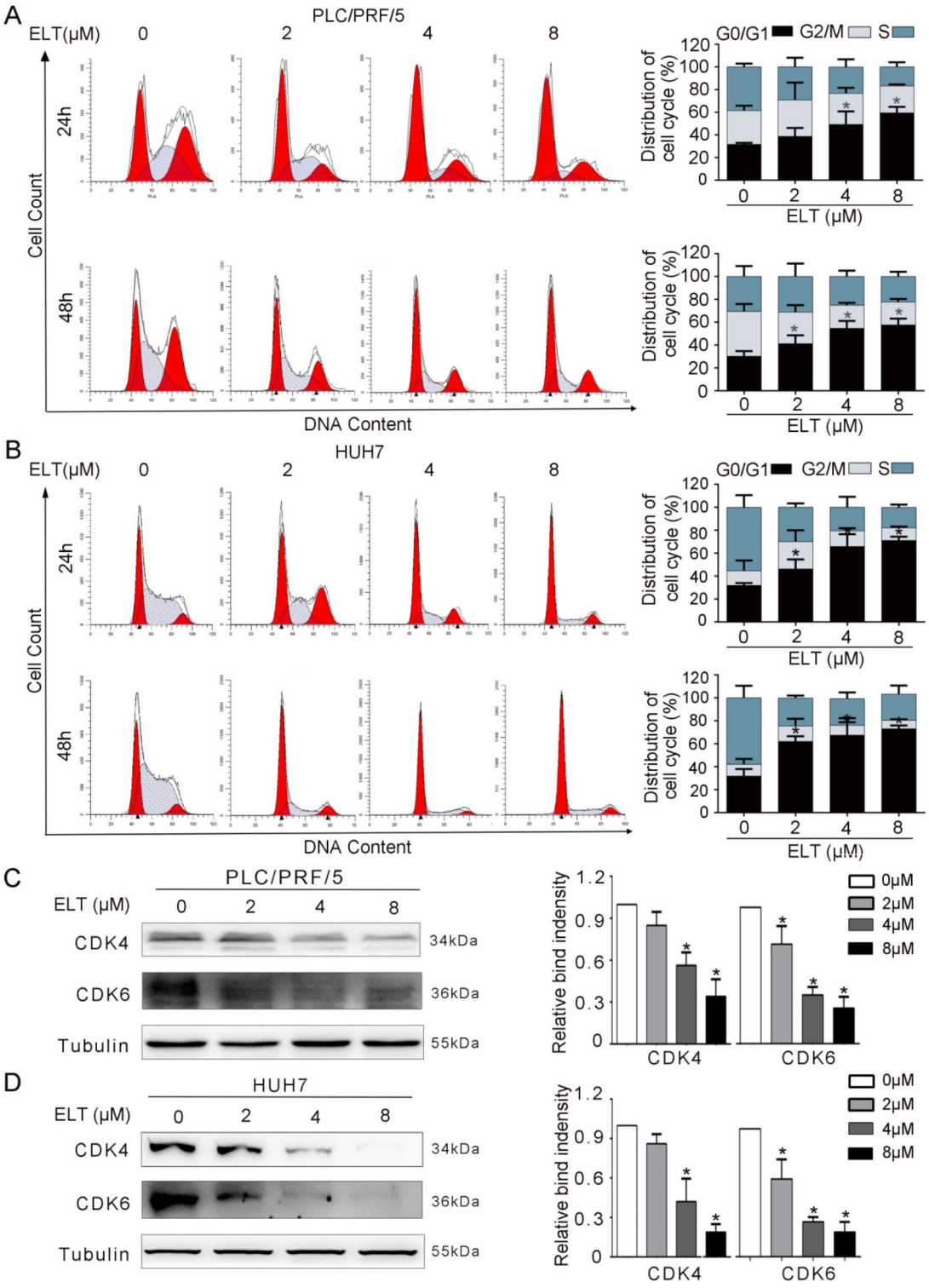

Fig. 2. ELT arrested PLC/PRF/5 and HUH7 cells at the G0/G1 phase. (**A**, **B**) Cell cycle distribution of PLC/PRF/5 and HUH7 cell lines after incubation with ELT at different concentrations for 24 h and 48 h. (**C**, **D**) The level of CDK4 and CDK6 proteins in the two cell lines after ELT treatment was detected by Western blotting. Tubulin served as an internal control. The samples derive from the same experiment, and the blots were processed in parallel. Data were presented as the average ± SD from three distinct experiments. * $p < 0.05$. Original blots were presented in Supplementary Fig S4.

findings, when considered in conjunction with those detailed in Sect. 3.1, indicate that the treatment of ELT has induced a reversible quiescent state in HCC cells.

ELT suppresses the β-catenin pathway in HCC cells

Given the well-established role of *β*-catenin in regulating the proliferation or quiescence of colorectal cancer cells[44], our focus shifted towards determining whether ELT could potentially interact with this protein, thus leading to the observed effects. Indeed, Western blotting analyses revealed a marked reduction in the content of *β*-catenin in its total, nuclear, and cytoplasmic forms within ELT-treated cells, exhibiting a concentration-dependent manner. This was also the case for the associated downstream proteins Cyclin D1, c-myc, and Survivin (Fig. 3).

Expression and GO/KEGG enrichment analyses of tsRNA in ELT-treated HCC cells

To investigate the potential correlation between tsRNA and the impact of ELT on PLC/PRF/5 cells, the cells were dosed with the drug at an 8 μM concentration for 48 h. Thereafter, an Arraystar small RNA microarray analyses was performed on the total RNA extract. The analyses revealed that 3,937 differentially expressed tsRNAs were generated, with 1,874 of these being up-regulated and 2,063 down-regulated. Nine tsRNAs that exhibited.

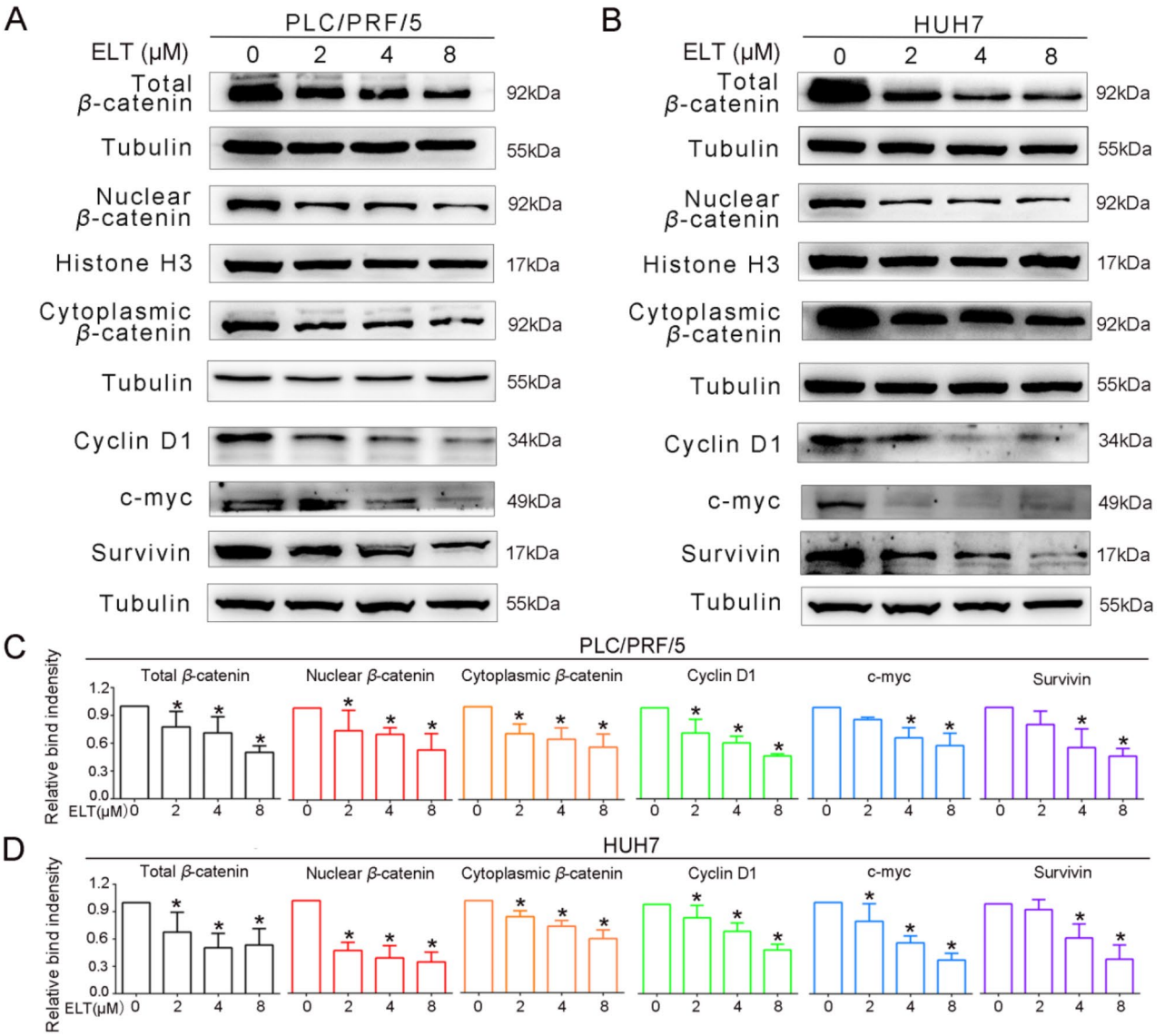

Fig. 3. ELT suppressed the *β*-catenin pathway in PLC/PRF/5 and HUH7 cells. (**A**, **B**) Western blotting results of *β*-catenin-related proteins in PLC/PRF/5 and HUH7 cells. (**C**, **D**) Quantification of the protein content of total, nuclear, and cytoplasmic *β*-catenin, Cyclin D1, c-myc, and Survivin in the two cell lines. Tubulin served as an internal control. Results were shown as the mean ± SD from three distinct experimental trials. $^{*}p < 0.05$. The samples derived from the same experiment, and the blots were processed in parallel. Original blots were presented in Supplementary Fig S5.

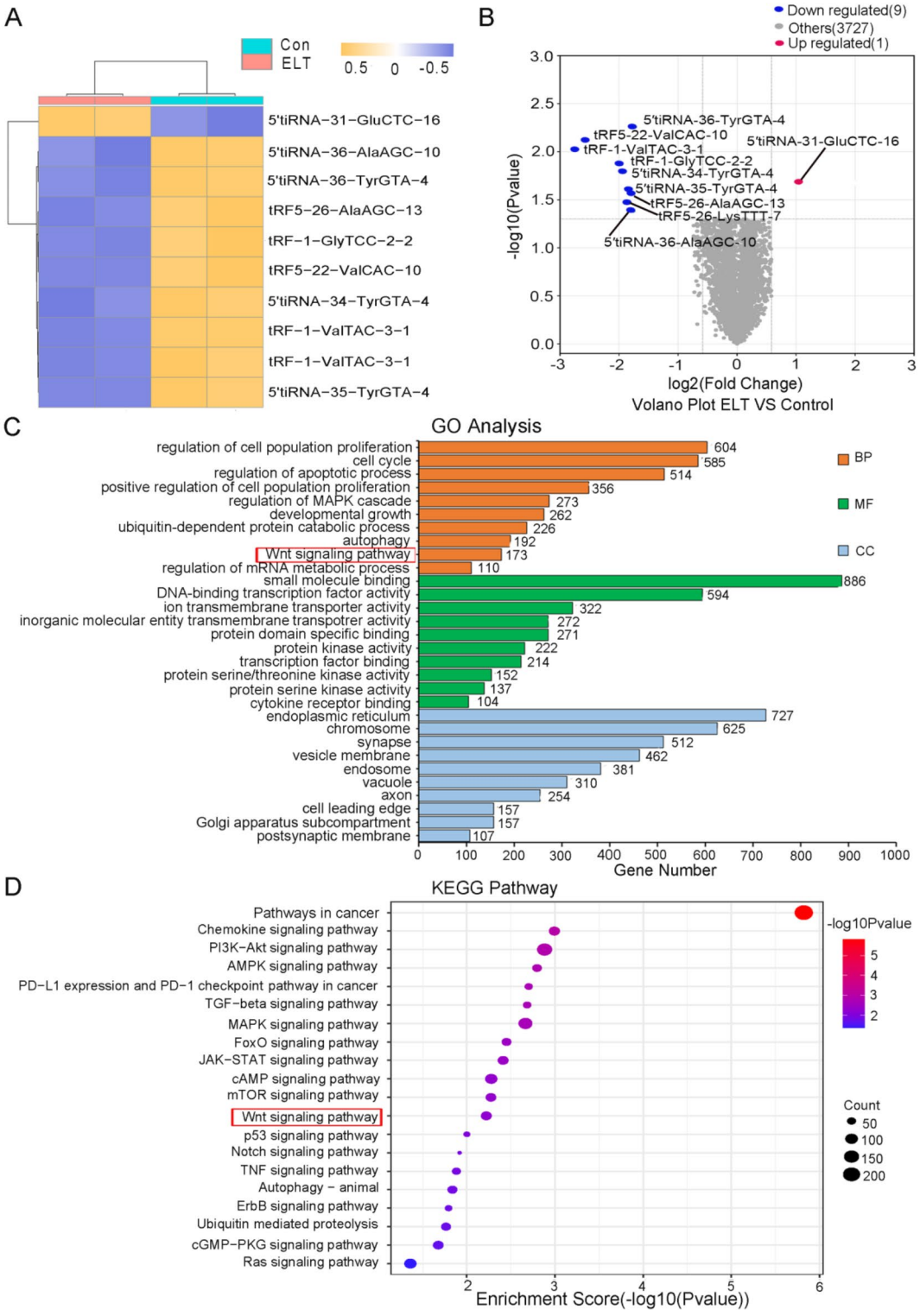

the most significant down-regulation, as indicated by the lowest fold change values, and one tsRNA that showed the most significant up-regulation, as indicated by the highest fold change value (p-value < 0.05), were selected for cluster analyses. The distribution of these ten tsRNAs was shown in a clustering heatmap in Fig. 4a, with orange indicating up-regulated ones and blue indicating down-regulated ones. In the corresponding volcano plot (Fig. 4b), the up-regulated ones were shown in red, and the down-regulated ones in blue. Their target genes were identified using GO and KEGG analyses. The GO terms that were notably enriched were predominantly categorized under BP, CC, and MF (Fig. 4c). Within the BP category, the target genes were chiefly associated with the modulation of cellular proliferation, cell cycle progression, apoptosis, autophagy, and the Wnt signaling pathway. Among the CCs, the main ones were associated with the postsynaptic membrane, the Golgi apparatus subcompartment, the cell leading edge, axons, and vacuoles. In the MFs, the main ones were associated with cytokine receptor binding, protein serine kinase activity, transcription factor binding, and

◀**Fig. 4**. Expression and GO/KEGG enrichment analyses of tsRNA in ELT-treated HCC. (**a**) Clustering heatmap of the differentially expressed genes of ten tsRNAs in the ELT and control groups. Orange represented up-regulated tsRNAs, and blue represented down-regulated tsRNAs in the groups. (**b**) The volcano plot displayed tsRNAs between the ELT and control groups. The blue dots represented the down-regulated tsRNAs, and the red dots represented the up-regulated tsRNAs. | FC > 1.5 |, p-value < 0.05. (**c**) GO analyses of predicted target genes of tsRNAs. (d) KEGG, developed by Kanehisa Laboratories[45], enriched the terms associated with the predicted target genes of tsRNAs in the ELT and control groups. (**e**) The diagram of 21 common genes at the intersection of Wnt and cancer pathways. These two pathways were referenced to Kanehisa et al.[46]. (**f**) The ranking chart of 21 common genes. (**g**) The relative expression level of tRF5-26-AlaAGC-13, 5'tiRNA-36-AlaAGC-10, tRF5-26-LysTTT-7, and 5'tiRNA-31-GluCTC-16 in PLC/PRF/5. U6 served as a control. (**h**, **i**) The level of DVL2 and DVL3 in two cell lines after a 48-h exposure to various concentrations of ELT by Western blotting. Tubulin served as a control. (**j**) The relative expression of DVL3 and DVL2 mRNA in PLC/PRF/5 cells after treating with tRF5-26-AlaAGC-13 or 5'tiRNA-36-AlaAGC-10 mimic. Results were expressed as mean ± SD of three independent experiments. *, $p < 0.05$; ns, $p > 0.05$. The samples derive from the same experiment, and the blots were processed in parallel. Original blots were presented in Supplementary Fig S6.

protein kinase activity. The KEGG analyses demonstrated that ELT impacted the MAPK, mTOR, Notch, and Wnt pathways, etc. (Fig. 4d). GO and KEGG analyses showed that the Wnt pathway (GO ID:0016055; Pathway ID: 04310) was the common pathway. Specifically, KEGG analyses identified 21 genes (DVL2, DVL3, WNT2, WNT3, FZD2, SMAD3, TCF7L2, WNT10A, WNT10B, WNT16, WNT2, WNT2B, WNT3, WNT3A, WNT4, WNT7A, WNT7B, WNT8B, and WNT11) that overlapped on the Wnt and cancer pathways (Fig. 4e). The genes were subsequently ranked based on their free-energy scores, as determined by the miRanda algorithm (Fig. 4f). The four most stable genes identified were DVL3, DVL2, WNT2, and WNT3. The corresponding tsRNAs were tRF5-26-LysTTT-7, 5'tiRNA-36-AlaAGC-10, 5'tiRNA-31-GluCTC-16, and tRF5-26-AlaAGC-13, respectively. Subsequently, the expression of tsRNA in PLC/PRF/5 cells was tested using RT-PCR. The data demonstrated a significant decrease in the levels of tRF5-26-AlaAGC-13 and 5'tiRNA-36-AlaAGC-10 as a result of ELT treatment, which supports the findings of the microarray analyses results. In contrast, the levels of tRF5-26-LysTTT-7 and 5'tiRNA-31-GluCTC-16 remained unchanged (Fig. 4g). Western blotting confirmed that the protein levels corresponding to tRF5-26-AlaAGC-13 and 5'tiRNA-36-AlaAGC-10 (viz. DVL3 and DVL2) had decreased significantly (Fig. 4h and i). To validate the relationship between the tsRNAs and their target genes, the mimics and negative control of tRF5-26-AlaAGC-13 and 5'tiRNA-36-AlaAGC-10 were transfected into PLC/PRF/5 cells[47]. It was observed that the tRF5-26-AlaAGC-13 mimic could increase the relative expression of DVL2 and DVL3 mRNA, and rescue their decrease induced by ELT. While the 5'tiRNA-36-AlaAGC-10 mimic could not increase either the relative expression of DVL2 or DVL3 mRNA, and rescue their decrease induced by ELT (Fig. 4j).

The characteristics of tRF5-26-AlAGC-13 (5′tRFAla)

According to the results in MINTbase v2.0 (http://cm.jefferson.edu/MINTbase/), tRF5-26-Ala-AGC-13 could be cleaved from three distinct mature tRNA precursors (tRNA-AlaAGC-22-1, tRNA-AlaAGC-13-1, tRNA-AlaAGC-13-2) as a 5'-tRF fragment (Fig. 5A). In the UCSC Genome Browser database, tRNA-AlaAGC-22-1 was located on chromosome 6p11.2 with coordinates of 58,141,877 – 58,141,949 and a length of 73 bp (Fig. 5B). tRNA-AlaAGC-13-1 was located on chromosome 6p22.2 with coordinates of 26,705,606 – 26,705,678 and a length of 73 bp (Fig. 5C). tRNA-AlaAGC-13-2 was located on chromosome 6p11.2 with coordinates of 58,164,628 – 58,164,700, and a length of 73 bp (Fig. 5D). The sequencing of mature tRNA revealed that the tRF5-26-AlaAGC-13 consists of 26 nt, which were identified as 5'-GGGGAATTAGCTCAAGCGGTAGAGCG-3'. The cleavage site was located at the end of the D-loop (CGCT) (Fig. 5E, F, and G). Using TargetScan and miRanda algorithms, we identified the binding site as a perfect match with both the DVL2 and DVL3 mRNA based on the secondary structure of tRNA, as shown in Fig. 5H. The site type between tRF5-26-AlaAGC-13 and DVL2 was 8mer-1a, with a perfect match between.

nucleotides 2 and 8. Similarly, the site type between tRF5-26-AlaAGC-13 and DVL3 was 7mer-1a, with their nucleotides 2–7 matching exactly. These findings may explain the lower binding energy between tRF5-26-AlaAGC-13 and DVL2 or DVL3. Following the nomenclature of Lyons et al.[48], we named tRF5-26-AlaAGC-13 as 5′tRF^{Ala}.

Discussion

Currently, the vast majority of clinically deployed small-molecule drugs exert their desired effects by binding to proteins. Given that merely 1.5% of the human genome is ultimately translated into protein, and with an estimated 20,000 human proteins, only 10–15% are linked to diseases, it is clear that the further development of protein-targeted drugs has obvious limitations[49]. Exacerbating matters, a significant number of disease-related proteins are considered to be "undruggable." As such, other targetable biomolecules are being sought more vigorously, with a particular focus currently being on the identification of small-molecule therapeutics that modulate human RNAs. Since 70–90% of the human genome is transcribed into RNA[50], and given that numerous RNAs can fold into three-dimensional structures, it is evident that these molecules, like proteins, should be amenable to selective targeting by small molecules[51]. Given their role as pivotal elements in the transfer of cellular information and the regulation of gene expression, the modulation of RNAs by small molecules presents an opportunity to therapeutically engage in a multitude of biological processes, even when downstream and "undruggable" protein targets are involved[52]. FDA-approved aminoglycosides, including

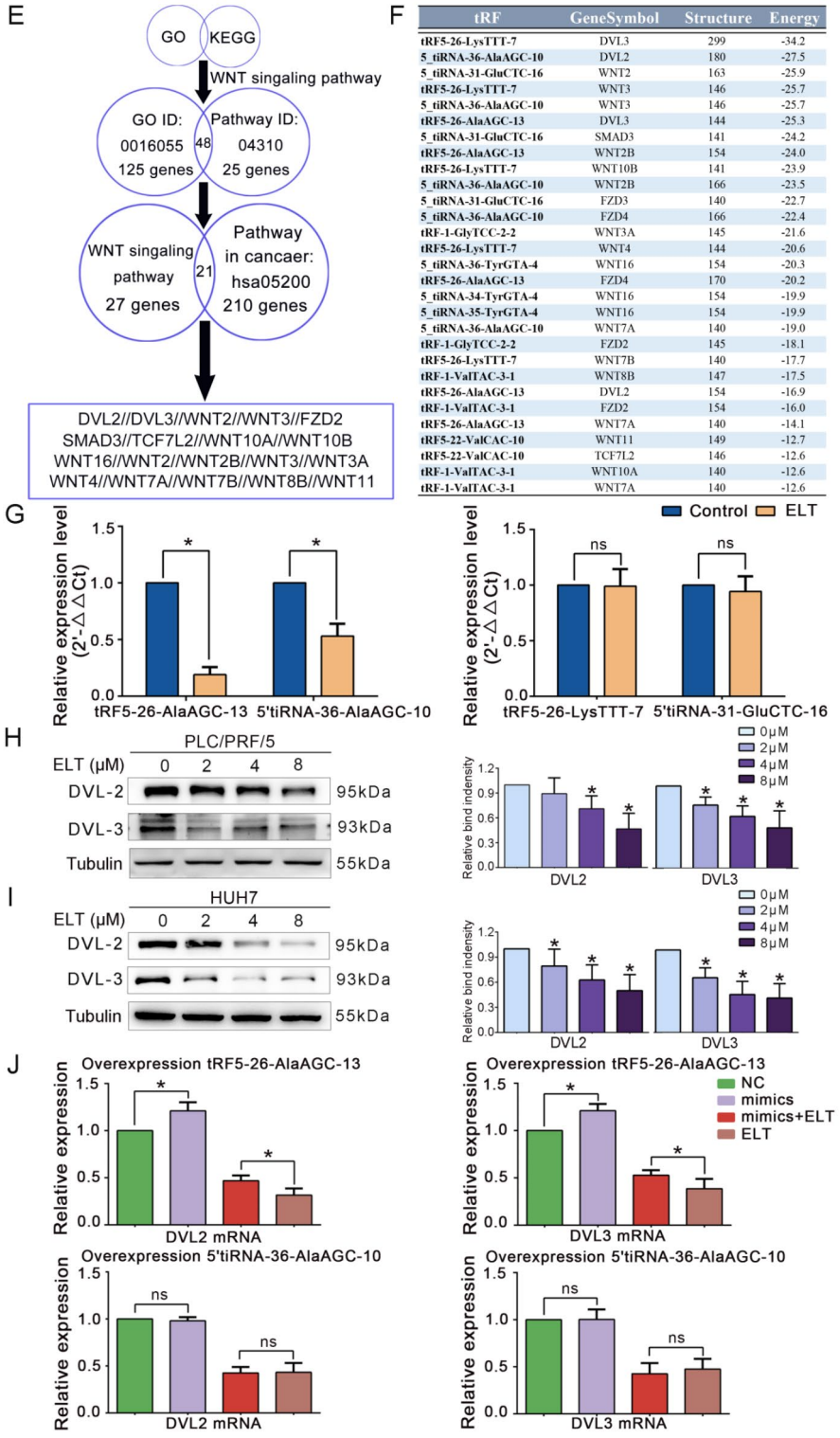

tRF	GeneSymbol	Structure	Energy
tRF5-26-LysTTT-7	DVL3	299	-34.2
5_tiRNA-36-AlaAGC-10	DVL2	180	-27.5
5_tiRNA-31-GluCTC-16	WNT2	163	-25.9
tRF5-26-LysTTT-7	WNT3	146	-25.7
5_tiRNA-36-AlaAGC-10	WNT3	146	-25.7
tRF5-26-AlaAGC-13	DVL3	144	-25.3
5_tiRNA-31-GluCTC-16	SMAD3	141	-24.2
tRF5-26-AlaAGC-13	WNT2B	154	-24.0
tRF5-26-LysTTT-7	WNT10B	141	-23.9
5_tiRNA-36-AlaAGC-10	WNT2B	166	-23.5
5_tiRNA-31-GluCTC-16	FZD3	140	-22.7
5_tiRNA-36-AlaAGC-10	FZD4	166	-22.4
tRF-1-GlyTCC-2-2	WNT3A	145	-21.6
tRF5-26-LysTTT-7	WNT4	144	-20.6
5_tiRNA-36-TyrGTA-4	WNT16	154	-20.3
tRF5-26-AlaAGC-13	FZD4	170	-20.2
5_tiRNA-34-TyrGTA-4	WNT16	154	-19.9
5_tiRNA-35-TyrGTA-4	WNT16	154	-19.9
5_tiRNA-36-AlaAGC-10	WNT7A	140	-19.0
tRF-1-GlyTCC-2-2	FZD2	145	-18.1
tRF5-26-LysTTT-7	WNT7B	140	-17.7
tRF-1-ValTAC-3-1	WNT8B	147	-17.5
tRF5-26-AlaAGC-13	DVL2	154	-16.9
tRF-1-ValTAC-3-1	FZD2	154	-16.0
tRF5-26-AlaAGC-13	WNT7A	140	-14.1
tRF5-22-ValCAC-10	WNT11	149	-12.7
tRF5-22-ValCAC-10	TCF7L2	146	-12.6
tRF-1-ValTAC-3-1	WNT10A	140	-12.6
tRF-1-ValTAC-3-1	WNT7A	140	-12.6

Figure 4. (continued)

neomycin, gentamicin, and streptomycin, have been recognized for decades as small molecules that block the bacterial ribosome, a ribosomal RNA and ribosomal protein complex, to inhibit bacterial protein production[53]. Similarly, the therapeutic efficacy of oxazolidinone antibiotics like linezolid and tedizolid is mediated through their interaction with the ribosome, preventing the assembly of the ribosomal-fMet-tRNA initiation complex[54]. Additionally, research has shown that small molecules can inhibit the viability, proliferation, migration, invasion, and epithelial-to-mesenchymal transition in diverse cancer cells by modulating miRNA levels in a direct or indirect manner. For instance, paeoniflorin is hypothesized to inhibit the proliferation and invasion

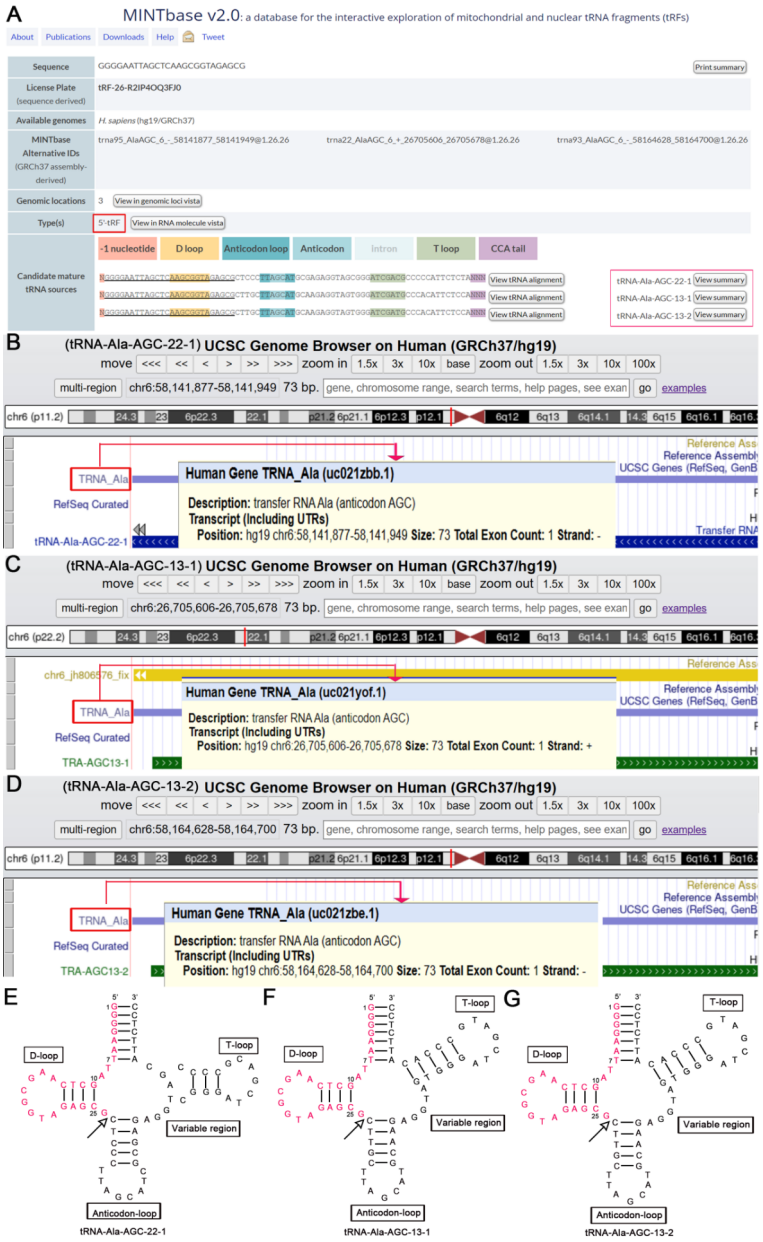

Fig. 5. The characteristics of tRF5-26-AlaAGC-13. (**A**) tRF5-26-AlaAGC-13 was a 5'tRF fragment of tRNA-Ala-AGC, derived from three mature tRNA precursors (tRNA-AlaAGC-22-1, tRNA-AlaAGC-13-1, tRNA-AlaAGC-13-2). (**B**) The genomic location of tRNA-AlaAGC-22-1 was identified as chromosome 6p12.2, spanning a length of 73 bp, as shown in the UCSC Genome Browser database. (**C**) The genomic location of tRNA-AlaAGC-13-1 was identified as chromosome 6p22.2, spanning a length of 73 bp, according to the UCSC Genome Browser database. To view further details of an item, simply click on it; this was indicated by the red arrows. (**D**) tRNA-AlaAGC-13-2 was located on chromosome 6p11.2, with a length of 73 bp, using the UCSC Genome Browser database. Details of the item could be displayed by clicking on it, as pointed out by the red arrows. (**E**-**G**) tRF5-26-AlaAGC-13 was derived from tRNA-AlaAGC-22-1, tRNA-AlaAGC-13-1, and tRNA-AlaAGC-13-2, which had a length of 26 nt. The cleavage site was located at the end of the D-loop sequence (CGCT). (H) tRF5-26-AlaAGC-13 showed a match with DVL2 or DVL3 mRNA. The symbol "|" indicated a perfect match. ":" indicated that a T: G or G: U match was made. 8mer-1a meant 3'-UTR matched exactly with nucleotide 2–8 nt of 5'tRF, and 1a represented the complementary pairing position of UTR and tRF5' where 1 nt was A. Local AU represented a region rich in AU, which was more likely to exert a biological function. The red bar indicated that the position was A: U, and that a greater degree of complementarity was preferable.

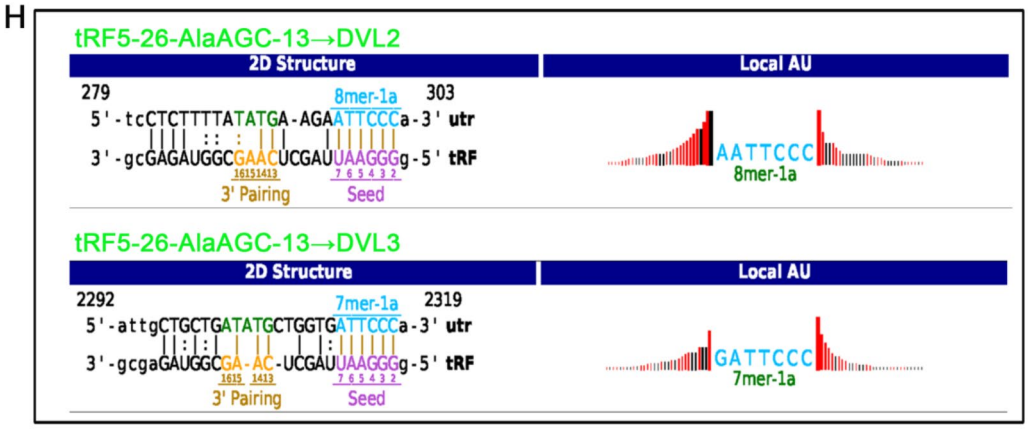

Figure 5. (continued)

of glioma cells by up-regulating miR-16[55]. Conversely, curcumin up-regulates the expression of the tumor suppressor miR-203 by interacting with the PI3K/AKT/mTOR signaling pathway, resulting in the suppression of cell proliferation and the induction of cell apoptosis in non-small cell lung cancer cells[56]. The drug propofol has been demonstrated to reduce inflammation, decrease oxidative stress, inhibit lung tissue apoptosis, improve lung function, and ameliorate pathological changes of lung tissue in a rat lung ischemia-reperfusion model. This is achieved through the regulation of miR-30b expression, which leads to the downregulation of Beclin-1 and inhibition of the JAK/STAT signaling pathway[57]. As with miRNAs, tsRNAs are reported to modulate various physiological processes. However, the potential disruption caused by small molecules in these processes has yet to be proven, let alone defined[58].

Eurycoma longifolia (EL), also known as "Tongkat Ali," is a globally renowned traditional herbal medicine, predominantly distributed in Southeast Asian countries. The roots and rhizomes of the plant have been used to treat a wide range of ailments, including sexual dysfunction, diabetes, rheumatism, infection, inflammation, anxiety, ulceration, and cancer[59]. The quassinoids of EL are regarded as the main bioactive constituents, exhibiting cytotoxic effects across a spectrum of cancer cell lines[60]. Of the 24 quassinoids tested, eurycomalactone (ELT) was identified as the most potent anti-proliferative agent, exhibiting an IC_{50} of 0.70 μM in colon 26-L5 cells, an IC_{50} of 0.59 μM in B16-BL6 cells, an IC_{50} of 0.78 μM in LLC cells, and an IC_{50} of 0.73 μM in A549 cells[61]. In this paper, we discovered that ELT can induce a state of quiescence in HCC PLC/PRF/5 and HUH7 cells. This is evident from its ability to arrest the cell cycle at the G0/G1 phase without resulting in cell death. Furthermore, it was observed that the cells retained the potential for reactivation after the withdrawal of ELT. The Wnt/β-catenin signaling pathway, linked to quiescence, is thought to be the pathway that is targeted by ELT. This is evidenced on the basis of the marked decrease in the expression of total, cytoplasmic, and nuclear β-catenin together with its target proteins c-myc, Survivin, and Cyclin D1 upon ELT exposure. To investigate the modulation of tsRNA connected to the β-catenin signaling pathway, an Arraystar small RNA microarray analyses was conducted on the total RNA solution extracted from PLC/PRF/5 cells following ELT treatment. Two new significantly reduced tsRNAs, namely 5′tiRNA^{Ala} and 5′tRF^{Ala}, were identified as being related to the upstream regulatory proteins of β-catenin, DVL2, and DVL3. The concentrations of these were found to be dramatically reduced by Western blotting. This conclusion is based on the well-established link between the 5′tiRNA^{Ala} and 5′tRF^{Ala} genetic sequence and DVL2 or DVL3 mRNA with low free energy scores and high structure scores[62]. To verify the relation between 5′tiRNA^{Ala} and 5′tRF^{Ala} and DVL2 and DVL3, we conducted an overexpression experiment by tsRNA mimics. Results showed that only the mimic of 5′tRF^{Ala} could increase DVL2 and DVL3 mRNA expression and rescue the decrease in expression induced by ELT. While the mimic of 5'tiRNA^{Ala} could not. The characteristics of 5′tiRNA-36-AlaAGC-10 (5′tiRNA^{Ala}) were shown in Fig S7. It has been demonstrated that the repression or activation effect of miRNAs on their target mRNAs is coordinated with the cell cycle. In actively dividing cells, they repress translation, whereas in non-dividing cells (quiescent and senescent cells), they perform activation[63–65]. Thus, if tsRNAs exert a similar effect to that of miRNAs, ELT may result in a reduction in DVL2 and DVL3 mRNA translation, leading to a subsequent decline in the levels of relevant proteins by diminishing the concentrations of 5′tRF^{Ala} in PLC/PRF/5 and HUH7 cells. Given that ELT resulted in HCC cell proliferation inhibition and cycle arrest at the G0/G1 phase, significantly switching them into a quiescent state. Taken together, the above-mentioned results demonstrate that the small-molecule natural product ELT inhibits the proliferation of HCC cells and does so by arresting the cell cycle at the G0/G1 phase. The resulting quiescent state, which is established reversibly, appears to result from ELT depressing the 5′tRF^{Ala}/DVL/β-catenin pathway.

Conclusions

The present study reported an interesting natural product, eurycomalactone, that can reversibly switch PLC/PRF/5 and HUH7 cells into a quiescent state, which is characterized by cell proliferation inhibition without cytotoxicity, cell cycle arrest at G0/G1 phase, and cell reactivation after ELT has been withdrawn. Western blotting results displayed that this quiescence was related to the depression of the Wnt/β-catenin pathway. Subsequent

small RNA microarray and bioinformatics analyses discovered a possibility that the significant decrease of two new tsRNAs, namely 5'tRF^{Ala} and 5'tiRNA^{Ala}, could suppress DVL2 and DVL3 mRNA translation, two pivotal upstream regulators of the Wnt/β-catenin signaling pathway. Moreover, overexpression experiment demonstrated that 5'tRF^{Ala} was related to DVL2 and DVL3 mRNA expression. Conclusively, our findings imply that tsRNAs, like miRNAs, might activate the translation of their matched mRNAs in quiescent cells and play a possible role in repressing tumor cell growth, although further evidence is still needed.

Data availability

The Arraystar small RNA microarray datasets presented in this study can be found in online repositories. The names of the repositories and accession number can be found below: Gene Expression Omnibus-GSE236560. Other data are contained within this article and the Supplementary File.

Received: 13 October 2024; Accepted: 14 January 2025
Published online: 24 March 2025

References

1. Romano, G., Veneziano, D., Acunzo, M. & Croce, C. M. Small non-coding RNA and cancer. *Carcinogenesis* **38**, 485–491 (2017).
2. Clamp, M. F. et al. Distinguishing protein-coding and noncoding genes in the human genome. *Proc. Natl. Acad. Sci. U.S.A* **104**, 19428–19433 (2007).
3. Gerstein, M. B. et al. What is a gene, post-ENCODE? History and updated definition. *Genome Res* **17**, 669–681 (2007).
4. Nicole Kresge, R. D. S., Robert, L. & Hill The purification and sequencing of alanine transfer ribonucleic acid: The work of Robert W. Holley. *J. Biol. Chem* **281**, e7–e9 (2006).
5. Liu, L. et al. Circular RNAs: Isolation, characterization and their potential role in diseases. *RNA Biol* **14**, 1715–1721 (2017).
6. Bartel, D. P., Metazoan & MicroRNAs *Cell* **173**, 20–51 (2018).
7. Girard, A., Sachidanandam, R., Hannon, G. J. & Carmell, M. A. A germline-specific class of small RNAs binds mammalian piwi proteins. *Nature* **442**, 199–202 (2006).
8. Carthew, R. W. & Sontheimer, E. J. Origins and mechanisms of miRNAs and siRNAs. *Cell* **136**, 642–655 (2009).
9. Taft, R. J. et al. Small RNAs derived from snoRNAs. *Rna* **15**, 1233–1240 (2009).
10. Chen, C. J. & Heard, E. Small RNAs derived from structural non-coding RNAs. *Methods* **63**, 76–84 (2013).
11. Shi, J., Zhou, T. & Chen, Q. Exploring the expanding universe of small RNAs. *Nat. Cell Biol* **24**, 415–423 (2022).
12. Zhang, Z., Zhang, J., Diao, L. & Han, L. Small non-coding RNAs in human cancer: Function, clinical utility, and characterization. *Oncogene* **40**, 1570–1577 (2021).
13. Fröhlich, K. S. & Vogel, J. Activation of gene expression by small RNA. *Curr. Opin. Microbiol* **12**, 674–682 (2009).
14. Chan, P. P. & Lowe, T. M. GtRNAdb 2.0: An expanded database of transfer RNA genes identified in complete and draft genomes. *Nucleic Acids Res* **44**, D184–D189 (2016).
15. Kirchner, S. & Ignatova, Z. Emerging roles of tRNA in adaptive translation, signalling dynamics and disease. *Nat. Rev. Genet* **16**, 98–112 (2014).
16. Grewal, S. S. Why should cancer biologists care about tRNAs? tRNA synthesis, mRNA translation and the control of growth. *Biochim. et Biophys. Acta (BBA) - Gene Regul. Mech* **1849**, 898–907 (2015).
17. Anderson, P. & Ivanov, P. tRNA fragments in human health and disease. *FEBS Lett* **588**, 4297–4304 (2014).
18. Suzuki, T., Nagao, A. & Suzuki, T. Human mitochondrial tRNAs: Biogenesis, function, structural aspects, and diseases. *Annu. Rev. Genet* **45**, 299–329 (2011).
19. Yao, P. & Fox, P. L. Aminoacyl-tRNA synthetases in medicine and disease. *EMBO Mol. Med* **5**, 332–343 (2013).
20. Balatti, V. et al. tsRNA signatures in cancer. *Proc. Natl. Acad. Sci* **114**, 8071–8076 (2017).
21. Du, J. et al. Biological function and clinical application prospect of tsRNAs in digestive system biology and pathology. *Cell Communication and Signaling* **21**, (2023).
22. Wen, J. et al. Research progress on the tsRNA classification, function, and application in gynecological malignant tumors. *Cell Death Discovery* **7**, (2021).
23. Wang, B., Yan, L., Xu, Q. & Zhong, X. The role of transfer RNA-Derived small RNAs (tsRNAs) in Digestive System tumors. *J. Cancer* **11**, 7237–7245 (2020).
24. Yang, M. et al. Transfer RNA-derived small RNAs in tumor microenvironment. *Molecular Cancer* **22**, (2023).
25. Aristeidis, G. et al. K.a.I. dissecting tRNA-derived fragment complexities using personalized transcriptomes reveals novel fragment classes and unexpected dependencies. *Oncotarget* **6**, 28 (2015).
26. Kim, H. K., Yeom, J. H. & Kay, M. A. Transfer RNA-Derived small RNAs: Another layer of gene regulation and novel targets for disease therapeutics. *Mol. Ther* **28**, 2340–2357 (2020).
27. Chu, X. et al. Transfer RNAs-derived small RNAs and their application potential in multiple diseases. *Front. Cell Dev. Biol* **10,** (2022).
28. Qin, C. X. et al. J.J. Pathological significance of tRNA-derived small RNAs in neurological disorders. *Neural Regeneration Res* **15,** (2020).
29. Lyons, S. M., Gudanis, D., Coyne, S. M., Gdaniec, Z. & Ivanov, P. Identification of functional tetramolecular RNA G-quadruplexes derived from transfer RNAs. *Nature Commun* **8,** (2017).
30. Tong, L. et al. The tRNA-derived fragment-3017A promotes metastasis by inhibiting NELL2 in human gastric cancer. *Fronti Oncol* **10,** (2021).
31. Wu, Y. L. et al. Z.-h. Epigenetic regulation in metabolic diseases: Mechanisms and advances in clinical study. *Signal Transduction and Targeted Therapy* **8**, (2023).
32. Weng, Q. et al. Extracellular vesicles-associated tRNA-derived fragments (tRFs): Biogenesis, biological functions, and their role as potential biomarkers in human diseases. *J. Mol. Med* **100**, 679–695 (2022).
33. Li, Y. et al. Stress-induced tRNA-derived RNAs: A novel class of small RNAs in the primitive eukaryote Giardia lamblia. *Nucleic Acids Res* **36**, 6048–6055 (2008).
34. Lee, Y. S., Shibata, Y., Malhotra, A. & Dutta, A. A novel class of small RNAs: tRNA-derived RNA fragments (tRFs). *Genes Dev* **23**, 2639–2649 (2009).
35. Li, S., Xu, Z. & Sheng, J. tRNA-derived small RNA: A novel regulatory small non-coding RNA. *Genes* **9**, 246 (2018).
36. Wang, J. H. et al. tsRFun: A comprehensive platform for decoding human tsRNA expression, functions and prognostic value by high-throughput small RNA-Seq and CLIP-Seq data. *Nucleic Acids Res* **50**, D421–D431 (2022).
37. Yao, D. et al. OncotRF: An online resource for exploration of tRNA-derived fragments in human cancers. *RNA Biol* **17**, 1081–1091 (2020).
38. Zhan, S. et al. Serum mitochondrial tsRNA serves as a novel biomarker for hepatocarcinoma diagnosis. *Front. Med* **16**, 216–226 (2022).

39. Kim, H. K. et al. A transfer-RNA-derived small RNA regulates ribosome biogenesis. *Nature* **552**, 57–62 (2017).
40. Zhu, L. et al. Exosomal tRNA-derived small RNA as a promising biomarker for cancer diagnosis. *Mol. Cancer* **18**, 1–5 (2019).
41. Balatti, V., Pekarsky, Y. & Croce, C. M. Role of the tRNA-Derived small RNAs in cancer: New potential biomarkers and target for therapy. *Adv. Cancer Res* **135**, 173 (2017).
42. Qinhu, W. T. et al. The tRNA-derived small RNAs regulate gene expression through triggering sequence-specific degradation of target transcripts in the Oomycete Pathogen Phytophthora sojae. *Front. Plant Sci* **07**, 1938 (2016).
43. Bates, R. B. & Tempesta, M. S. Structures of eurycomalactone and related terpenoids. *J. Org. Chem* **49**, 2820–2821 (1984).
44. Lo, Y. H. et al. SPDEF induces quiescence of colorectal cancer cells by changing the transcriptional targets of β-catenin. *Gastroenterology* **153**, 205–218e208 (2017).
45. Minoru Kanehisa, S. G. KEGG: Kyoto Encyclopedia of genes and genomes. *Nucleic Acids Res* **28**, 27–30 (2000).
46. Kanehisa, M., Furumichi, M., Sato, Y., Kawashima, M. & Ishiguro-Watanabe, M. KEGG for taxonomy-based analysis of pathways and genomes. *Nucleic Acids Res* **51**, D587–D592 (2023).
47. Yang, Z. et al. Systematic analysis of tRNA-derived small RNAs reveals therapeutic targets of Xuefu Zhuyu decoction in the cortexes of experimental traumatic brain injury. *Phytomedicine* **102**, (2022).
48. Lyons, S. M., Achorn, C., Kedersha, N. L., Anderson, P. J. & Ivanov, P. YB-1 regulates tiRNA-induced stress granule formation but not translational repression. *Nucleic Acids Res* **44**, 6949–6960 (2016).
49. Warner, K. D., Hajdin, C. E. & Weeks, K. M. Principles for targeting RNA with drug-like small molecules. *Nat. Rev. Drug Discovery* **17**, 547–558 (2018).
50. Dunham, I. K., Anshul, Aldred, Shelley, F. Collins, Patrick, Davis, J., & Carrie, A. An integrated encyclopedia of DNA elements in the human genome. *Nature* **489**, 57–74 (2012).
51. O'Rourke, J. R. & Swanson, M. S. Mechanisms of RNA-mediated disease. *J. Biol. Chem* **284**, 7419–7423 (2009).
52. Falese, J. P., Donlic, A. & Hargrove, A. E. Targeting RNA with small molecules: From fundamental principles towards the clinic. *Chem. Soc. Rev* **50**, 2224–2243 (2021).
53. Schroeder, R. & Wank, W. C. Modulation of RNA function by aminoglycoside antibiotics. *EMBO J* **19**, 1–9 (2000).
54. Zhanel, G. G. et al. Tedizolid: A novel oxazolidinone with potent activity against multidrug-resistant gram-positive pathogens. *Drugs* **75**, 253–270 (2015).
55. Wang, X. Z. et al. The multifaceted mechanisms of Paeoniflorin in the treatment of tumors: State-of-the-art. *Biomed. Pharmacother* **149**, 112800 (2022).
56. Saini, S. et al. Curcumin modulates MicroRNA-203–Mediated regulation of the src-akt Axis in bladder cancer. *Cancer Prev. Res* **4**, 1698–1709 (2011).
57. Kang, H., Chen, J. & Cao, S. Propofol regulates the expression of BecliN-1 through miR-30b and protects against Lung Ischemia-Reperfusion Injury. *Cell. Mol. Biol* **67**, 348–355 (2022).
58. Lin, Y. et al. Effects of dexmedetomidine on the expression profile of tsRNAs in LPS-induced acute lung injury. *Journal of Clinical Laboratory Analysis* **36**, (2021).
59. Thu, H. E., Hussain, Z., Mohamed, I. N. & Shuid, A. N. Recent advances in antibacterial, antiprotozoal and antifungal trends of *Eurycoma longifolia*: A review of therapeutic implications and future prospects. *Curr. Drug Targets* **19**, 1657–1671 (2018).
60. Duan, Z. K. et al. Quassinoids: Phytochemistry and antitumor prospect. *Phytochemistry* **187**, (2021).
61. Miyake, K., Li, F., Tezuka, Y., Awale, S. & Kadota, S. Cytotoxic activity of quassinoids from Eurycoma Longifolia. *Nat. Prod. Commun* **5**, 1009–1012 (2010).
62. Mo, D. et al. A tRNA fragment, 5′-tiRNAVal, suppresses the Wnt/β-catenin signaling pathway by targeting FZD3 in breast cancer. *Cancer Lett* **457**, 60–73 (2019).
63. Truesdell, S. S. et al. MicroRNA-mediated mRNA translation activation in quiescent cells and oocytes involves recruitment of a nuclear microRNP. *Sci. Rep* **2,** (2012).
64. Vasudevan, S. & Tong, Y. S. J. A. switching from repression to activation: MicroRNAs can Up-Regulate translation. *Science* **318**, 1931–1934 (2007).
65. Zhang, X. et al. MicroRNA directly enhances mitochondrial translation during muscle differentiation. *Cell* **158**, 607–619 (2014).

Author contributions

Conceptualization, X.W. and H.B.L.; methodology, Z.P.Z. and Y.M.W; software, Z.P.Z., W.Q.L. and W.X.Y.; validation, Z.P.Z., W.Q.L. T.G. and B.W.; formal analyses, Z.P.Z. and W.Q.L.; investigation, Z.P.Z., Y.M.W., W.Q.L., Z.X.L., Y.C.L., B.M.; and M.Y.S.; resources, Z.P.Z., Z.F.L., X.X.X., W.X.Y. and D.L.L.; data curation, Z.P.Z.; writing—original draft preparation, Z.P.Z. and X.W.; writing—review and editing, X.W. and H.B.L.; visualization, X.W., H.B.L. and H.L.M.; supervision, M.Z.Z. and H.L.M.; project administration, X.W. and H.B.L.; funding acquisition, H.L.M., X.W. and M.Z.Z. All authors have read and agreed to the published version of the manuscript.

Funding

This work was supported by the Science and Technology Planning Project of Zhangjiang Municipality (Grant no. 2021A05092, 2021A05097 and 2022A01148), the Discipline Construction Project of Guangdong Medical University (Grant no. GDMXK2021002, GDMXK2021003), the Science and Technology Planning Project of Shenzhen Municipality (Grant no. JCYJ20190806154207168), and the Key Research Laboratory and Key Discipline Development Project for Traditional Chinese Medicine in the Prevention and Treatment of Infectious Diseases of Traditional Chinese Medicine Bureau of Guangdong Province (Grant no.2023337) and the Talent Development Foundation of The First Dongguan Affiliated Hospital of Guangdong Medical University (Grant no. GCC2023022).

Declarations

Competing interests

The authors declare no competing interests.

Institutional Review Board Statement

Not applicable.

Informed consent

Not applicable.

Additional information

Supplementary Information The online version contains supplementary material available at https://doi.org/10.1038/s41598-025-86888-x.

Correspondence and requests for materials should be addressed to M.Z., H.M. or X.W.

Reprints and permissions information is available at www.nature.com/reprints.

Publisher's note Springer Nature remains neutral with regard to jurisdictional claims in published maps and institutional affiliations.